Static structure of active Brownian hard disks

IOP Publishing Journal of Physics: Condensed Matter
J. Phys.: Condens. Matter **30** (2018) 074001 (11pp) https://doi.org/10.1088/1361-648X/aaa3bf

Static structure of active Brownian hard disks

N de Macedo Biniossek[1], H Löwen[1], Th Voigtmann[1,2] and F Smallenburg[1,3]

[1] Institut für Theoretische Physik II: Weiche Materie, Heinrich Heine-Universität Düsseldorf, Universitätsstraße 1, 40225 Düsseldorf, Germany
[2] Institut für Materialphysik im Weltraum, Deutsches Zentrum für Luft- und Raumfahrt (DLR), 51170 Köln, Germany
[3] Laboratoire de Physique des Solides, CNRS, Univ. Paris-Sud, Univ. Paris-Saclay, 91405 Orsay, France

E-mail: thomas.voigtmann@dlr.de

Received 11 October 2017, revised 18 December 2017
Accepted for publication 22 December 2017
Published 19 January 2018

Abstract

We explore the changes in static structure of a two-dimensional system of active Brownian particles (ABP) with hard-disk interactions, using event-driven Brownian dynamics simulations. In particular, the effect of the self-propulsion velocity and the rotational diffusivity on the orientationally-averaged fluid structure factor is discussed. Typically activity increases structural ordering and generates a structure factor peak at zero wave vector which is a precursor of motility-induced phase separation. Our results provide reference data to test future statistical theories for the fluid structure of active Brownian systems.

This manuscript was submitted for the special issue of the *Journal of Physics: Condensed Matter* associated with the Liquid Matter Conference 2017.

Keywords: active colloids, active Brownian particles, active hard disks, Brownian dynamics simulations, fluid structure

(Some figures may appear in colour only in the online journal)

1. Introduction

Active Brownian particles (ABP) are a widely used model system to study the statistical physics of swimming microorganisms [1–3]. In the ABP model, particles undergo Brownian translational and rotational motion, and in addition possess an 'active' mechanism of self-propulsion along a fixed body axis. The simplest such model is that of active hard spheres (AHS), where particle interactions are spherically symmetric and only enforce no-overlap conditions. In particular, no direct interactions between the swimming directions of AHS exist. Despite this simplification, AHS still show interesting non-equilibrium phase behavior that allows to investigate many principles of actively driven systems. They can also be realized to good approximation in experiments on colloidal 'Janus' particles [4–6].

For equilibrium ('passive') fluids, the basic quantity revealing the structural correlations in the disordered fluid state is the structure factor $S(q)$, or alternatively the radial pair-distribution function $g(r)$ [7]. Since the early days of liquid state physics, the structure factor has been measured by scattering experiments and computed by simulations and integral equation theory. In this respect the hard-sphere system (including its two-dimensional version of hard disks) has played a pivotal role to understand fluid structure and to test approximative theories. The hard-sphere potential does not have an energy scale and therefore, temperature is irrelevant in determining the phase behavior. This allows to examine the role of structural correlations in fluids most clearly. The structural properties of active fluids have been much less studied (but see [8] for a recent exception). This is a significant gap, because the homogeneous active fluid can provide a clear-cut testing ground to extend the well-established concepts of classical statistical physics to regions far from thermal equilibrium.

In this contribution, we provide reference simulation data for the static structure factor $S(q)$ and the pair distribution function $g(r)$ of active Brownian hard disks in two spatial

dimensions. As stated above, hard-sphere like interactions are the least arbitrary starting point to describe sterical repulsion between particles, and in equilibrium fluids, the approach to start from hard spheres and extend to other types of interactions has been hugely successful. In active fluids, there might be a subtle interplay between the softness of repulsion and active driving [8], so that it is important to establish the hard-sphere reference case. We restrict ourselves to two-dimensional systems for simplicity. To date, most experiments on Janus colloids are done in quasi-2D settings, and many simulation studies of the phase behavior of ABP have also been performed in 2D. Brownian dynamics simulations of strict hard disks are not straightforward as already known from passive systems (see e.g. [9–11]) so special care is needed for the algorithm used. Here we choose an event-driven scheme [11] which is particularly designed to be efficient for Brownian hard disks.

Sufficiently strong self propulsion induces clustering of ABP, so that for a large range of densities, ABP systems evolve into inhomogeneous states of very dense clusters separated by very dilute regions [12, 13]. This phenomenon is called motility-induced phase separation (MIPS) as it shares a number of qualitative features with the liquid–gas phase separation known from equilibrium fluids. MIPS has been studied in great detail for various spherical ABP models with different interactions between the particles [14–16], since recently also including the hard-sphere case (using the same simulation algorithm as ours) [17]. Here we deliberately restrict our attention to the homogeneous fluid state outside the spinodal of MIPS.

2. Methods and techniques

The active Brownian hard-disk system obeys the following equations of motion for the positions $\vec{r}_j$ and the orientation angles θ_j of the particles (relative to a fixed laboratory coordinate frame):

$$\mathrm{d}\vec{r}_j = \sqrt{2D_\mathrm{t}}\,\mathrm{d}\vec{W}_j + v_0\vec{e}(\theta_j)\,\mathrm{d}t, \qquad |\vec{r}_j - \vec{r}_k| \geqslant \sigma\ \forall j,k, \tag{1a}$$

$$\mathrm{d}\theta_j = \sqrt{2D_\mathrm{r}}\,\mathrm{d}W_j^\theta. \tag{1b}$$

Here, $j = 1,\ldots N$ labels the particles. Brownian translational and rotational diffusion is described by uncorrelated Wiener processes $\mathrm{d}\vec{W}_j$ and $\mathrm{d}W_j^\theta$; their amplitude is given by the translational diffusion coefficient D_t and the rotational diffusion coefficient D_r. Self propulsion is modeled by a fixed swimming speed v_0 along the particles orientation, $\vec{e}(\theta) = (\cos\theta, \sin\theta)^T$. The hard-sphere interactions translate into no-overlap conditions $|\vec{r}_j - \vec{r}_k| \geqslant \sigma$ for all particle pairs.

The hard-core diameter σ and the translational diffusion coefficient D_t are used to set the units of length and time in the following. There remain three parameters to specify the state of the system: the density $n = N/V$, expressed as a dimensionless packing fraction $\eta = (\pi/4)n\sigma^2$, the self-propulsion velocity v_0 (in units of D_t/σ), and the rotational diffusion coefficient D_r (in units of D_t/σ^2). For 3D passive hard spheres, the Stokes–Einstein relation fixes $D_\mathrm{r} = 3D_\mathrm{t}/\sigma^2$, assuming Stokes flow in the solvent and stick boundary conditions on the particle surface. However, for active systems, the effective rate of change of particle orientations may be significantly different from this passive value, depending on the swimming mechanism. We will therefore fix $D_\mathrm{r} = 1$ as a reference case for most simulations, and also explore the effect of changes in D_r, i.e. changes in the persistence of active motion.

Given the particle positions, one obtains the static structure factor,

$$S(q) = \frac{1}{N}\left\langle \sum_{j,k=1}^{N} \mathrm{e}^{-\mathrm{i}\vec{q}\cdot(\vec{r}_j - \vec{r}_k)} \right\rangle, \tag{2}$$

where the angular brackets denote an average over the non-equilibrium stationary state, and $\vec{q}$ is the wave vector of the density fluctuations that are probed by $S(q)$. Note that in the homogeneous, isotropic fluid, $S(q)$ depends on $\vec{q}$ only through its magnitude $q = |\vec{q}|$. The static structure factor is intimately related to the radial distribution function $g(r)$ defined by

$$g(r) = \frac{1}{nN}\left\langle \sum_{j\neq k} \delta(\vec{r} - (\vec{r}_j - \vec{r}_k)) \right\rangle, \tag{3}$$

which quantifies the probability density for finding a particle at distance r from a given particle, irrespective of their orientations. Again, $g(r)$ quantifies structural properties of the isotropic homogeneous fluid, although for ABP systems, the angle-resolved pair distribution function provides further information [8].

In addition to $S(q)$ and $g(r)$, we quantify the emergence of clusters in low-density systems by measuring cluster size distributions. Here, two particles are considered to be part of the same cluster if their center-to-center distance is smaller than $r_c = 1.5\sigma$. This value is a reasonable estimate of the first minimum in $g(r)$ for the entire regime of investigated parameters. We obtain cluster size distributions by calculating a histogram of the number N_n of clusters of size n in the system, averaged over many configurations. We then define the average cluster size $\langle n\rangle$ for a randomly chosen particle as

$$\langle n\rangle = \left\langle \frac{1}{N}\sum_{i=1}^{N} n_i \right\rangle, \tag{4}$$

where n_i is the size of the cluster particle i is in, and the angular brackets denote an average over many configurations.

Finally, we measure the global hexagonal bond order parameter ψ_6

$$\psi_6 = \frac{1}{N}\left| \sum_{i=1}^{N} \frac{1}{N_b} \sum_{j=1}^{N_b} e^{6i\theta_{ij}} \right|, \tag{5}$$

where N_b is the number of nearest neighbors (i.e. particles within a distance $r_c = 1.5\sigma$), and θ_{ij} is the angle between the $\hat{\mathbf{x}}$-axis and the vector connecting particle i to one of its nearest neighbors j. This parameter is 1 for a perfect hexagonal crystal, and close to 0 in an isotropic fluid.

Simulations were carried out using an event-driven Brownian dynamics (ED-BD) algorithm [11]. In the ED-BD simulation, a fixed 'Brownian' time step Δt is introduced,

and at each time step, Gaussian trial displacements $\Delta\vec{r}_i$ and angle increments $\Delta\theta_i$ are drawn for all the particles. The self-propulsion term is included by drawing the $\Delta\vec{r}_i$ from appropriately shifted Gaussians. To propagate the system to the next time steps, the trial displacements have to be modified to avoid particle overlaps. This is done by assigning to the particles pseudo-velocities $\vec{v}_i = \Delta\vec{r}_i/\Delta t$, and by performing event-driven molecular dynamics using these pseudo-velocities in the time interval $[t, t + \Delta t]$. This way, the ED-BD algorithm guarantees no-overlap conditions at any time, and thus incorporates hard-sphere interactions exactly.

In the passive case, the ED-BD algorithm has been shown to accurately describe the Brownian motion of hard spheres, if the time step is reasonably small, $\Delta t < 0.1\,\sigma^2/D_\mathrm{t}$, say [11]. Note however that for strong self-propulsion and/or fast reorientational diffusion, significantly smaller time steps may be required. The extension to active particles has been used to study glassy dynamics of dense AHS systems [18], and more recently also MIPS [17].

We performed runs with $N = 1000$ and $N = 5000$ particles to estimate finite-size effects. These are found to be small for the structural quantities we study for state points sufficiently far from the spinodal of MIPS. Results are shown for the $N = 5000$ system. The Brownian time step was chosen to be $\Delta t = 0.001\,\sigma^2/D_\mathrm{t}$, and some runs with $\Delta t = 0.01\,\sigma^2/D_\mathrm{t}$ were performed to confirm that no significant finite-time step effects remain in $S(q)$. From individual runs with a specific choice of parameters, after an initial transient time of $t_i = 333\,\sigma^2/D_\mathrm{t}$ to reach a stationary state, 133 configurations in $[t_i, t_f]$ with $t_f = 1000\,\sigma^2/D_\mathrm{t}$ were stored and analyzed to obtain $S(q)$ and $g(r)$. To obtain $S(q)$, a set of 5000 $\vec{q}$-vectors compatible with periodic boundary conditions were used to evaluate equation (2), which were afterwards binned according to $|\vec{q}|$. For $g(r)$, bins of width $0.01\,\sigma$ were used in evaluating equation (3).

3. Results

3.1. Passive hard disks

We begin by recalling the features of the passive reference system. The only relevant parameter in the passive hard-disk system is the packing fraction η. Hard disks are known to order at high densities, transforming first from the fluid to a hexatic phase, and later to a crystalline phase. The nature and phase-transition boundaries of the fluid–hexatic and the hexatic–solid transitions have only recently become clear in large-scale simulations [19] and experiments [20]: in the regime $0.700 \leqslant \eta \leqslant 0.716$, coexistence between a fluid and the hexatic phase was found. There is a further continuous transition to a solid at $\eta \simeq 0.720$. In the following, we will restrict the discussion to packing fractions $\eta \leqslant 0.7$.

The static structure factor of the fluid displays the standard features known from simple fluids (figure 1): with increasing packing fraction, intermediate-range order in the fluid becomes more pronounced, and this gives rise to damped oscillations in $S(q)$ that become increasingly pronounced. The ordering is reflected in a pronounced first of $S(q)$ at $q_* \approx 6/\sigma$ (for $\eta = 0.6$). The position of this peak (or rather, the period of the oscillations) reflects a typical interparticle distance. The sharpness of the peak is an indicator for how pronounced ordering is.

For 3D hard spheres, several well known approximation schemes exist for $S(q)$. For example, a widely used analytical, albeit approximate, expression is the Percus–Yevick (PY) structure factor [7]. In 2D, no closed analytical form of the PY approximation for $S(q)$ is known. An empirical expression has been proposed by Baus and Colot [21]. The Baus–Colot expression provides an excellent description of the data, as shown by the dashed lines in figure 1.

3.2. Active hard disks

We now turn to the discussion of the active hard-disk system with rotational diffusivity $D_\mathrm{r} = 1$. For self-propulsion velocities v_0 that are below the onset of motility-induced phase separation (estimated to be around $v_0 = 12$ in the present system [17]), a similar evolution of $S(q)$ with increasing packing fraction is seen as in the passive system. This case is shown in figure 2 for $v_0 = 10$.

In particular the evolution of the first and second peaks in $S(q)$ does not differ qualitatively from the one in the passive system. For $\eta = 0.7$, the second peak around $q\sigma = 12$ exhibits an asymmetric shape, which we interpret as a precursor of incipient ordering. It is known that two-dimensional ABP systems crystallize at high densities (seen, for example, in active hard-core Yukawa systems [22]). For the hard-disk case discussed here, the passive system displays much stronger signatures of ordering in $S(q)$ at $\eta = 0.7$ than the active system does. This is consistent with the expectation that—at least for self-propulsion velocities small enough to prevent MIPS—the ordering transition sets in at higher densities in the presence of active motion.

The main difference of the active $S(q)$ to the passive one is in the low-q behavior. At densities comparable to the critical density of MIPS, a strong increase of $S(q \to 0)$ is seen in the active system. This is the signature of impending phase separation that is expected from the analogy with equilibrium systems. Precursors of this low-q increase are seen at all densities shown in figure 2.

The structure factors shown in figure 2 are exemplary for the active hard-disk fluid. At higher v_0, only the low-density regime remains, because MIPS sets in; our simulations confirm that phase separation prevails for large v_0 up to very high densities. It is therefore, at least for $D_\mathrm{r} \approx 1$, not possible to prepare a homogeneous monodisperse hard-disk fluid for large v_0 and large η.

To understand the effect of activity on the static structure of the fluid, it is instructive to discuss cuts in parameter space where the packing fraction is fixed. Increasing the self-propulsion velocity v_0 for a low-density system ($\eta = 0.2$ shown in figure 3(a)) causes two prominent changes: first, the main peak of $S(q)$ shifts to larger q and increases in amplitude (and the subsequent peaks undergo a similar change). The increase of the peaks in $S(q)$ signals that structural order in the more

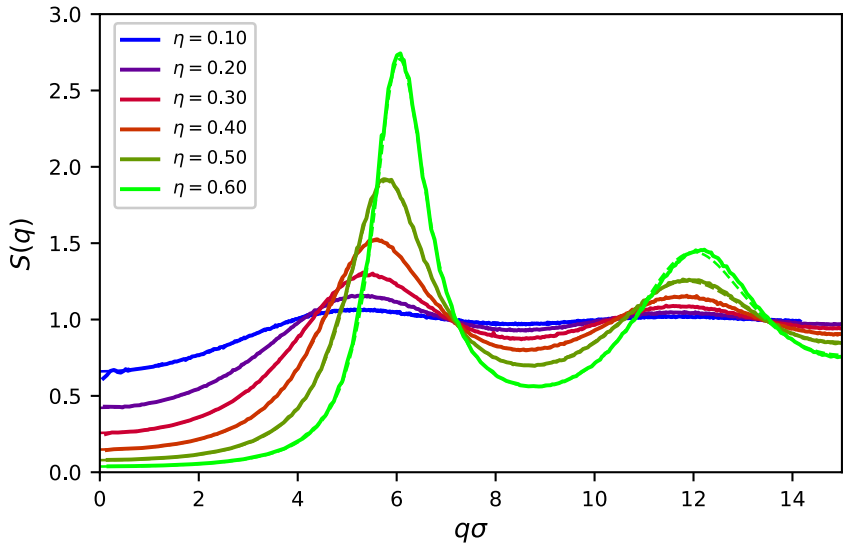

Figure 1. Static structure factor $S(q)$ of passive hard-disk systems with packing fractions $\eta = 0.1$, 0.2, 0.3, 0.4, 0.5, and 0.6 (top to bottom around $q\sigma = 2$). Solid lines: results from ED-BD simulations. Dashed lines represent the Baus–Colot expression for $S(q)$.

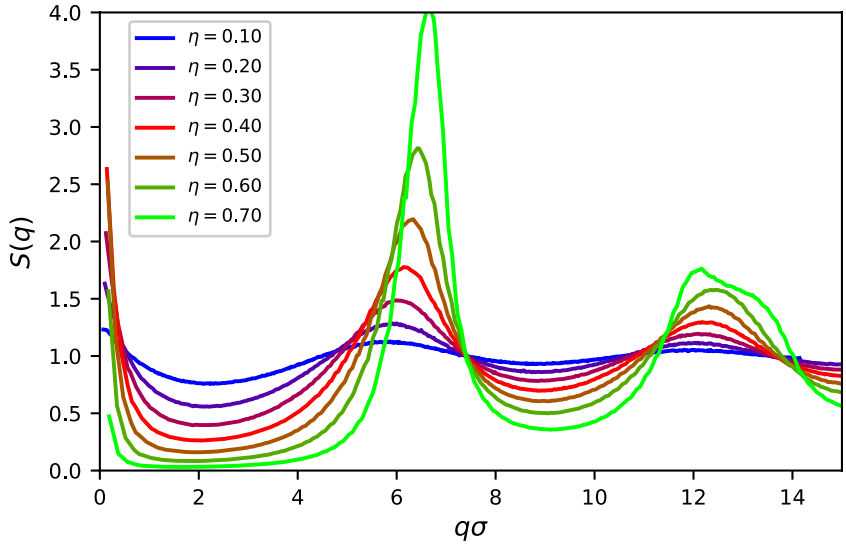

Figure 2. Static structure factor $S(q)$ of active Brownian hard disks with self-propulsion velocity $v_0 = 10\,D_t/\sigma$ and rotational diffusion coefficient $D_r = 1\,D_t/\sigma^2$, for packing fractions $\eta = 0.1$, 0.2, 0.3, 0.4, 0.5, 0.6, and 0.7.

active fluid is more pronounced, while the shift to larger q indicates that the average particle distance is reduced. This is consistent with a visual inspection of the simulation snapshots illustrated in figure 3(b), which shows the formation of local areas with both higher ordering and density.

Second, the low-q region of $S(q)$ increases with increasing self-propulsion speed. This latter effect is attributed to the emergence of a phase-separated region, as discussed above. If one defines the isothermal compressibility κ_T of the active fluid system in terms of the particle-number fluctuations by extending the well-known equilibrium relation, $\kappa_T = S(q \to 0)/nk_BT$ (where k_BT is the thermal energy needed to define an energy scale for the compressibility), to the non-equilibrium stationary state, the active fluid is much more compressible than the passive one.

Interestingly, the $S(q)$ appear to approach a limiting curve for large v_0: in figure 3(a), the strongest change is seen upon increasing v_0 from zero to about 10, while a further increase by a factor of 10 (up to $v_0 = 100$) only causes small further changes in the average fluid structure. Also the MIPS spinodal is nearly vertical in the v_0-versus-η plane [17], indicating that there is a regime where self-propulsion effects saturate. The shift in the peak positions of $S(q)$ indicate that the average particle distance decreases from about $2\pi/5\,\sigma \approx 1.26\,\sigma$ to about $2\pi/6\,\sigma \approx 1.05\sigma$. Hence, the saturation may stem from the fact that for true hard disks, a further increase in activity cannot cause particles to stay closer than σ on average. The saturation effect may thus be masked for soft spheres.

The radial distribution function $g(r)$ provides more intuitive information on the average structure. At the low density discussed here, $\eta = 0.2$, the equilibrium $g(r)$ is relatively featureless: it shows a weak enhancement over the ideal-gas value at particle contact, but quickly decays to unity for larger r. Increasing v_0 for the low-density system leads to a strong

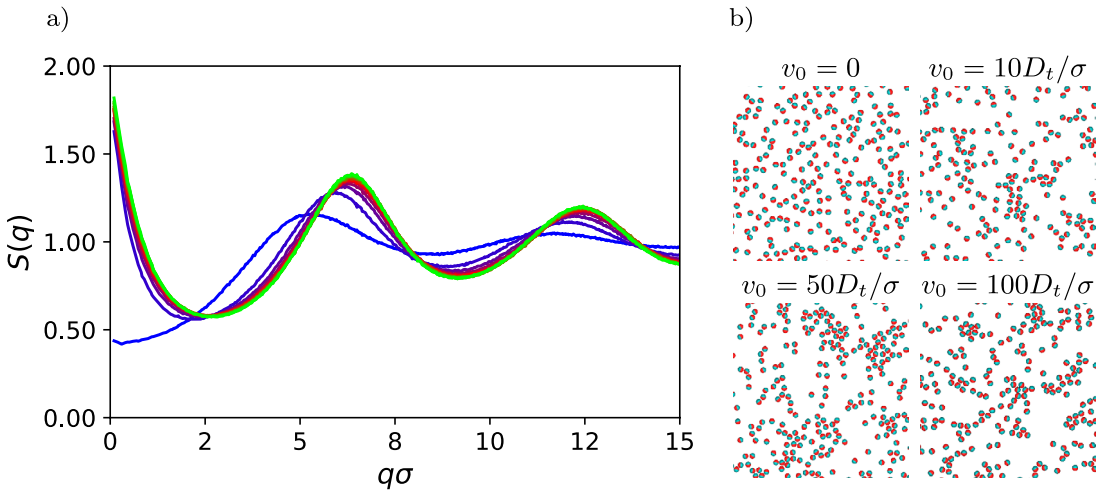

Figure 3. (a) Low-density fluid regime: static structure factor $S(q)$ for active hard disks with $D_r = 1\,D_t/\sigma^2$ and at packing fraction $\eta = 0.2$. Different curves corresond to different self-propulsion velocity: $v_0 = 0\,D_t/\sigma$ to $v_0 = 100\,D_t/\sigma$ increasing in steps of 10 (blue to green). (b) Simulation snapshots at the indicated self-propulsion velocities. The self-propulsion of each particle is directed towards its red side. Note that the total simulation box is significantly larger than the region depicted here.

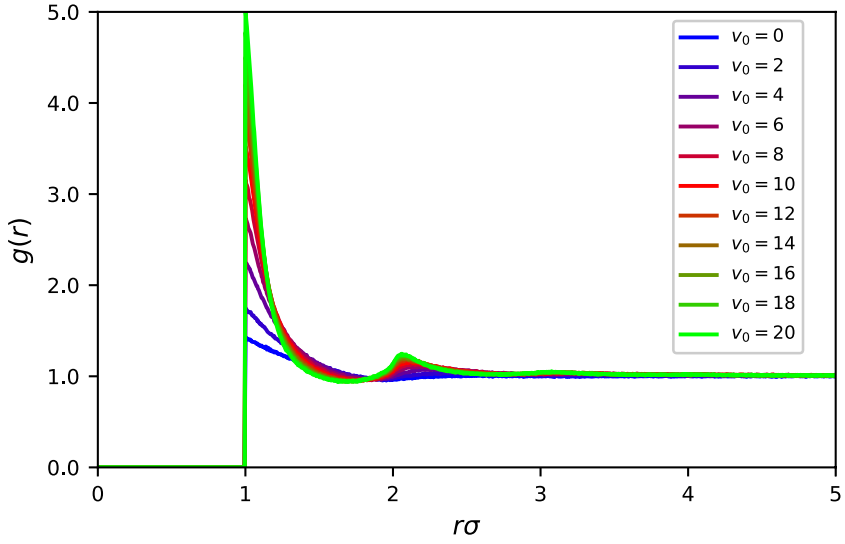

Figure 4. Radial distribution function $g(r)$ of an active Brownian hard-disk system at packing fraction $\eta = 0.2$, for self-propulsion velocities $v_0 \in [0, 20]$ (in steps of two, from bottom to top at $r = 1^+$).

enhancement of $g(r)$ near contact, see figure 4. This is in line with the interpretation that the average particle distance decreases with increasing self-propulsion velocity.

At sufficiently large v_0 there emerges a second peak around $r = 2\sigma$. Hence, active particles form small transient clusters. However, no pronounced peaks are seen at $r \approx n\sigma$ with $n > 2$. Thus, the system does not (yet) form large clusters with a statistically significant probability, and it also does not form pronounced intermediate-range order. This observation is confirmed by examining the distribution of cluster sizes in the system at different self-propulsion velocities (see figure 5). Regardless of the value of v_0, the number density ρ_n of clusters of size n decays exponentially with n for sufficiently large clusters. With increasing v_0, the average cluster size any particle is in (shown in the inset) increases from approximately 4 particles to 13, consistent with the emergence of a shell of next-nearest neighbors in the $g(r)$.

The changes in $g(r)$ that are visible in figure 4 can be contrasted to those found in ABP systems with soft interactions [23]. There, a comparable change of v_0 only led to a relatively mild change in $g(r)$, and the main effect was a shift of the nearest-neighbour peak to smaller distances.

An appealing concept is to map activity onto an effective interaction between the particles. Quite robustly for a number of different ABP models, activity induces effective attractions that become increasingly strong when v_0 is increased [23–26]. For soft-sphere ABP, the interaction range was found to be around 20% of a particle diameter at moderate densities [23].

To describe the effects of attractions in passive colloidal systems, the square-well system (SWS) is a canonical starting point [27]. In this model, a hard-sphere repulsion is supplemented by an attraction of fixed strength Γ and range $\delta\sigma$. For the 3D SWS, the static structure factor $S(q)$ can be obtained analytically within the mean-spherical approximation for δ

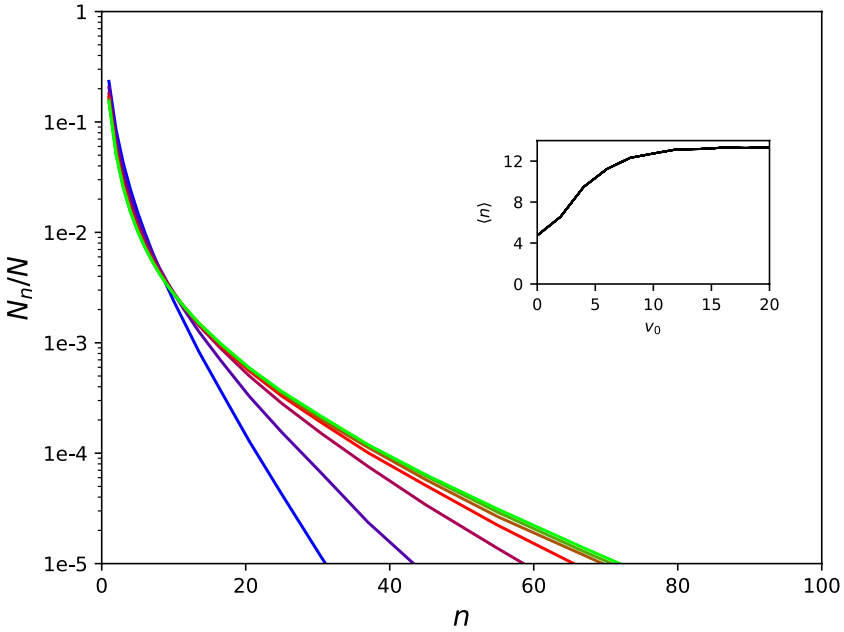

Figure 5. Cluster size distributions of systems with packing fraction $\eta = 0.2$ for self-propulsion velocities $v_0 \in [0, 20]$ (in steps of two, from bottom to top). The inset shows the typical cluster size $\langle n \rangle$ (defined as the average cluster size associated with a randomly chosen particle) as a function of v_0.

not too large [28]. At low density, the SWS-$S(q)$ displays a change upon increasing the attraction strength Γ that is similar to the one seen for the low-density AHS in figure 3: increasing attraction causes increased structural order, and a shift of the average particle separation to lower distances. This confirms earlier findings that activity can be mapped to an effective attraction in describing the fluid structure [24]. The mapping $v_0 \leftrightarrow \Gamma$ is however quite nonlinear, because the saturation effect we find for the AHS upon increasing v_0 is not found in the SWS upon increasing Γ.

We now turn to the high-density fluid, limited to small enough v_0 so that the system remains homogeneous. As the phase diagram confirms [17], there opens a small window where the system is not yet crystallized and not yet phase-separated. We discuss two packing fractions for this case, $\eta = 0.6$ and $\eta = 0.7$. The latter case represents the upper end of the equilibrium fluid regime in passive hard disks, and the structure functions for this system already show precursors of a phase transition to the hexatic phase.

The $S(q)$ at high densities, figure 6, demonstrate an interesting trend upon increasing v_0 that is absent at low densities: while the main peak of $S(q)$ monotonically shifts to the right with increasing v_0, it first weakens, and then increases with v_0. The corresponding effect in $g(r)$ is an interplay between a sharpening of the contact-value peak and an increasing depletion of the region between the first neighboring shells. However, this structural change is too subtle to be clearly visible in the simulation snapshots. The initial decrease in the amplitude of $S(q)$ is much more pronounced at $\eta = 0.7$, but already noticable at $\eta = 0.6$, where precursors of hexatic ordering are not yet obvious. We therefore attribute the non-monotonic change to a genuine change in the way activity influences the fluid structure, and not to the vicinity of a phase transition.

In figure 7, we show the full behavior of the position and height of the main peak as a function of η and v_0. Note that at $\eta = 0.5$ and lower, the peak height monotonically increases with v_0. The sharp increases in peak position and height for strongly active particles at high packing fraction are associated with the formation of crystalline regions. This is consistent with the increase of $\langle \psi_6 \rangle$ observed in this regime, shown in figure 7(c).

The non-monotonic trend revealed in figures 6 and 7 indicates that the effect of activity in the high-density hard-disk system is twofold: first, activity reduces ordering in the dense system. This is also expected from simulation studies of glassy dynamics, where a shift of the glass transition to higher densities with increasing activity was seen [18]. Similar trends are confirmed for various other model systems [29, 30] and predicted by theory [31]. Such a 'fluidization' of the system is usually associated with a weakening of the peak amplitudes in $S(q)$. It is reminiscent of the reentrant melting of glass-forming systems with short-ranged attraction, where a similar decrease of peak height in $S(q)$ with increasing attraction strength describes the structural changes of the system [28]. Second, stronger activity in the high-density system restores the effects that also prevail at lower densities. Here, activity favors structural order. For the case we study here, the crossover between the two effects occurs around $v_0 = 5\, D_t/\sigma$, slightly depending on the packing fraction.

Again, the comparison with the passive square-well system allows to understand the qualitative mapping of activity to effective interactions. Specifically, the non-monotonic change in the first peak of $S(q)$ allows to estimate the range of the effective attraction. For the SWS with an attraction range of, say, $\delta = 20\%$, the same trend is found at large densities as it was also found in the low-density state: increasing attraction strength Γ increases the peak height and shifts its

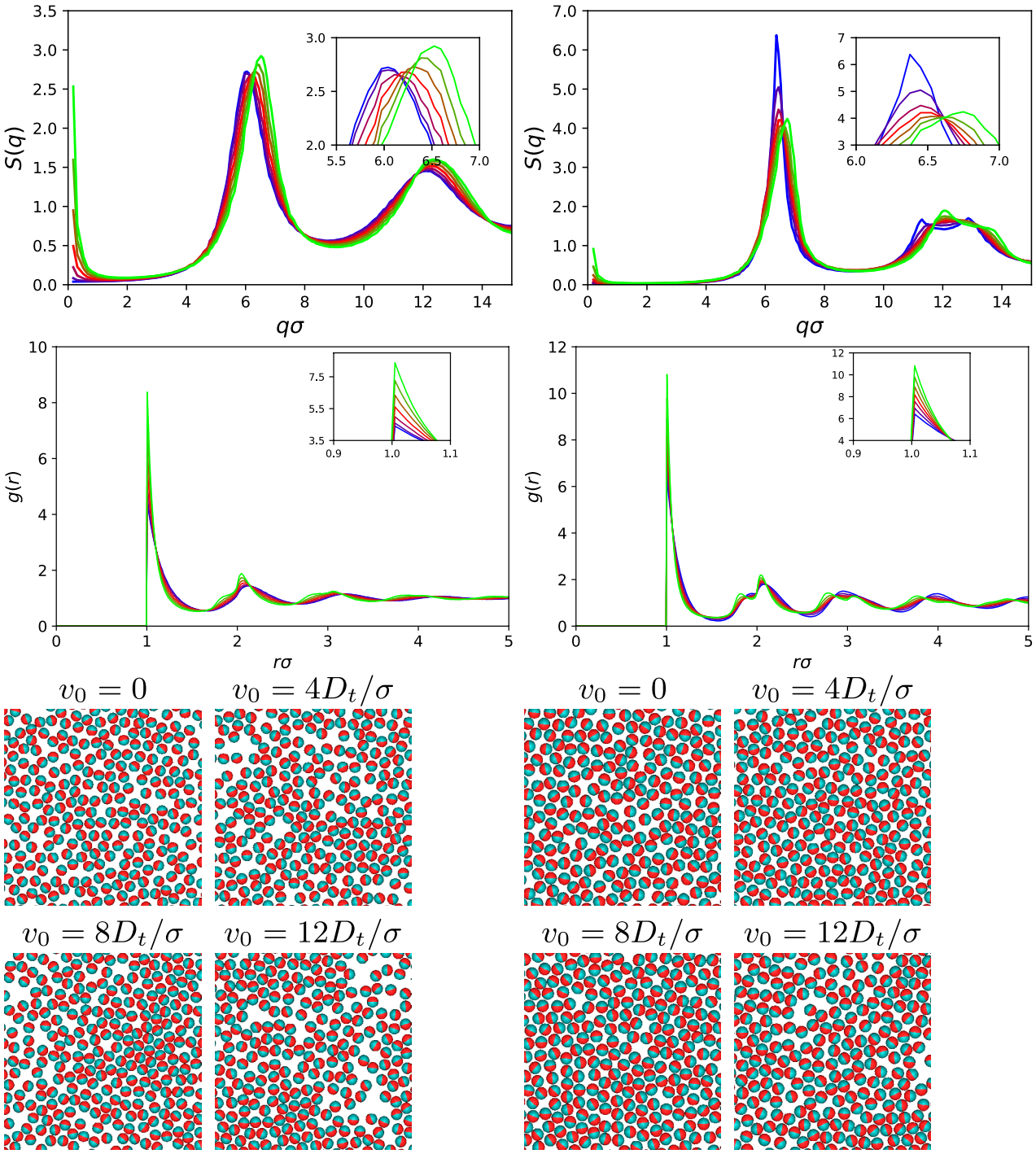

Figure 6. High-density fluid regime: static structure factor $S(q)$ (top row), radial distribution function $g(r)$ (middle row), and snapshots (bottom row) of active hard disks with packing fraction $\eta = 0.6$ (left column) respectively $\eta = 0.7$ (right column). Different curves correspond to different self-propulsion speeds $v_0 = 0$, 2, 4, 6, 8, 10, 12 (from blue to green; curves ordered by increasing first-peak position in $S(q)$ from left to right).

position to larger q (recall figure 3). The situation changes however, if one considers short-ranged attractions. For, say, $\delta = 10\%$, the dense SWS reproduces a decrease in peak height with increasing Γ up to about $\Gamma = 5\,k_\mathrm{B}T$, followed by an increase upon further increasing Γ. (To exemplify this, figure 8 shows the corresponding $S(q)$ for a 3D $S(q)$, evaluated in the mean-spherical approximation [28].) From this similarity in trends one may conclude that indeed, activity in the AHS can be mapped to an effective attraction, of a range around 10%. The SWS also offers a physical explanation for the different behavior of $S(q)$ at high densities as compared to low densities: at $\eta \approx 0.6$, the average particle separation is on the order of 10% of a particle diameter. If the attraction range and the interparticle separation are comparable, the effect of increasing attraction strength is to increase disorder, because some particles will be bounded more strongly, while others

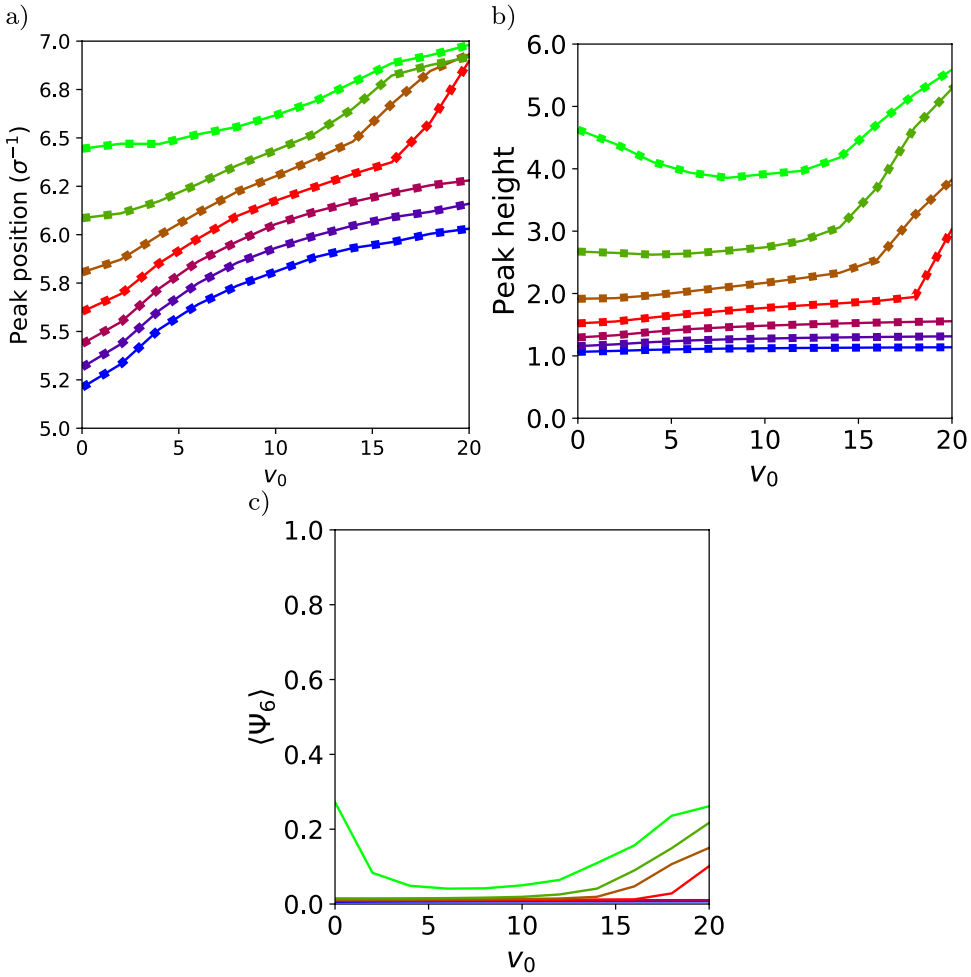

Figure 7. (a) and (b): Position (left) and height (right) of the main peak in the structure factor of active Brownian particles with $D_r = 1\, D_t/\sigma^2$, as a function of self-propulsion speed. Different lines indicate different packing fractions, ranging from $\eta = 0.1$ (bottom) to 0.7 (top) in steps of 0.1. (c) Global hexagonal bond order parameter $\langle \psi_6 \rangle$ for the same parameters.

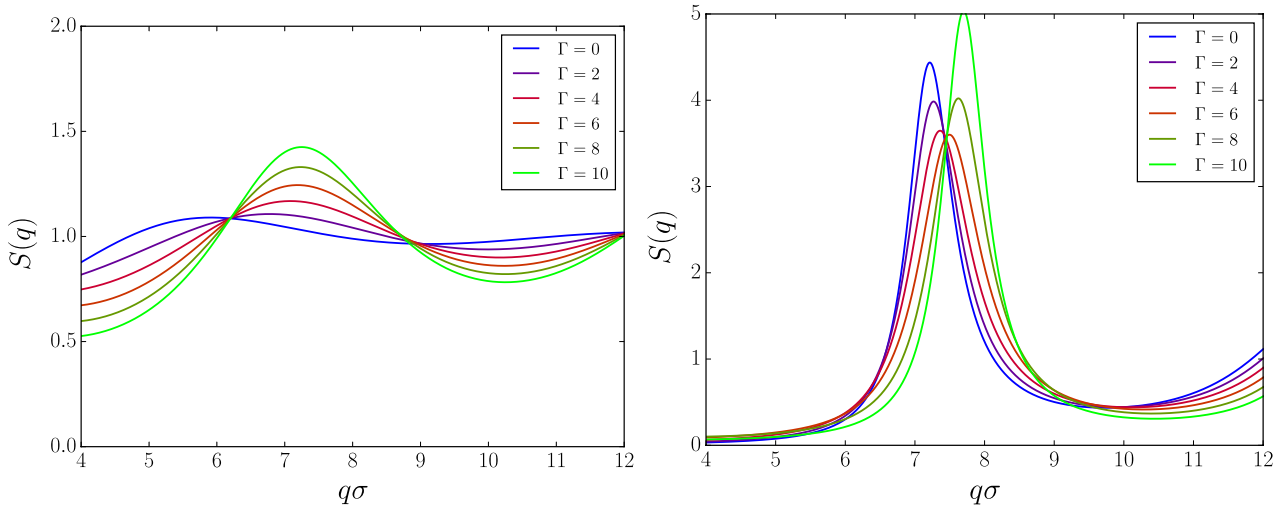

Figure 8. Static structure factor $S(q)$ of a 3D square-well system with short-ranged attraction (range 0.1σ), as a function of attraction strength ($\Gamma = 0$, 2, 4, 6, 8, and 10; blue to green), for moderate density (left panel; 3D packing fraction $\varphi = 0.1$) and for high density (right panel; $\varphi = 0.55$).

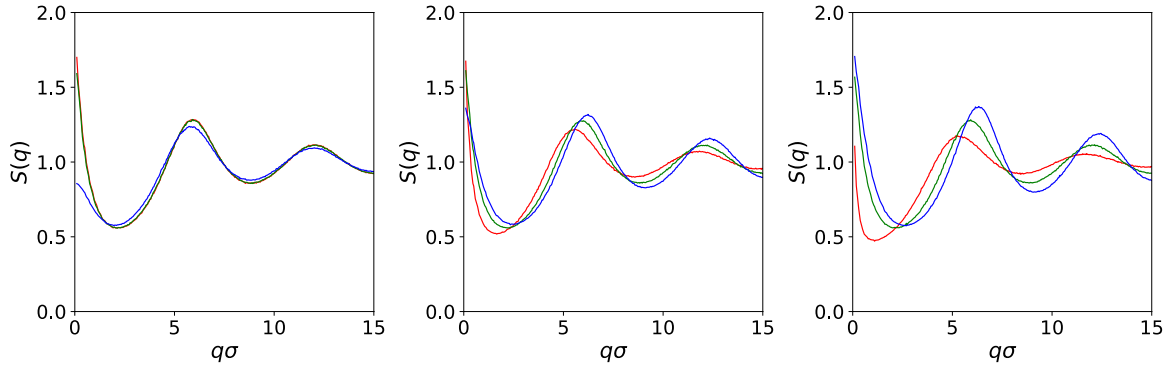

Figure 9. Static structure factor of active hard-disks fluid at packing fraction $\eta = 0.2$ with different rotational diffusion coefficients $D_r = 0.1$, 1, and 10 (red, green, blue). Left: comparison at constant self-propulsion velocity (translational Péclet number) $\mathrm{Pe_t} = v_0\sigma/D_t = 10$; middle: comparison at constant Péclet number $\mathrm{Pe} = v_0^2/D_rD_t = 100$; right: comparison at constant persistence length (rotational Péclet number) $\mathrm{Pe_r^{-1}} = v_0/\sigma D_r = 10$.

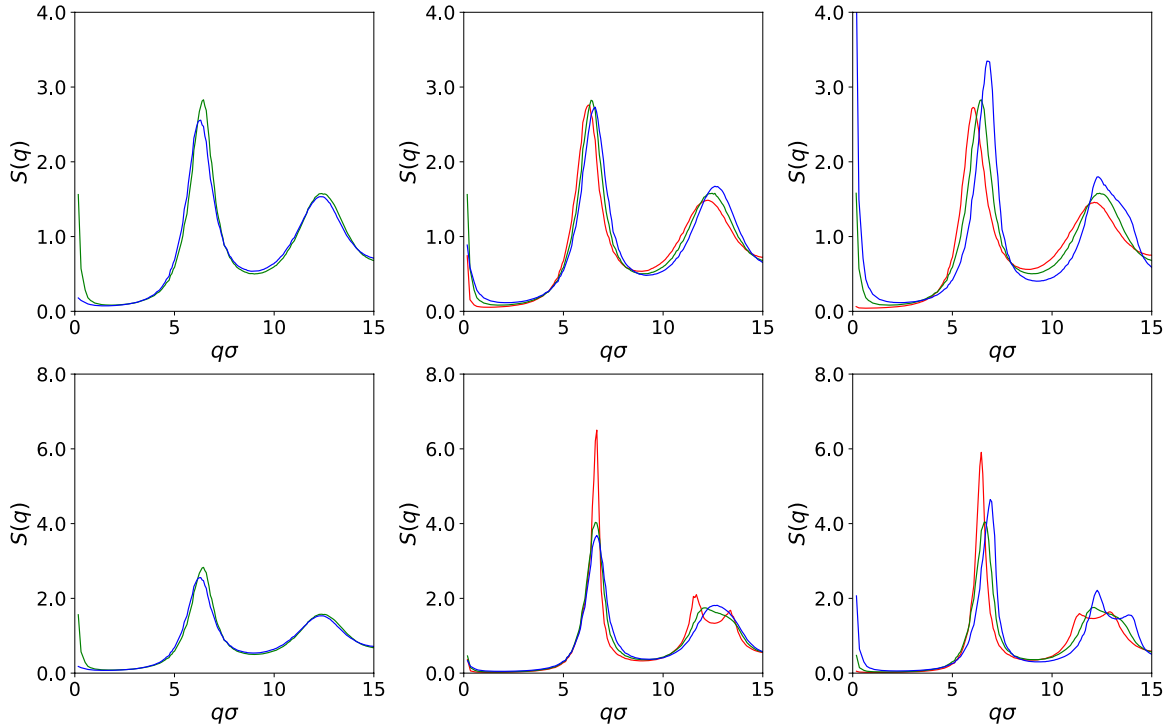

Figure 10. Static structure factor of active hard-disks fluid at packing fraction $\eta = 0.6$ (top row) respectively $\eta = 0.7$ (bottom row) with different rotational diffusion coefficients $D_r = 0.1$, 1, and 10 (red, green, blue), at constant $\mathrm{Pe_t} = 10$ (left), constant $\mathrm{Pe} = 100$ (middle), and constant $\mathrm{Pe_r^{-1}} = 10$ (right). Results are omitted for the state point ($\mathrm{Pe_t} = 10$, $D_r = 0.1$), where the system is already phase separated.

can explore a larger configuration-space volume. Only if the attraction is sufficiently strong, the energetic increase in order offsets the entropic decrease.

3.3. Influence of rotational persistence

Activity induces a coupling between D_r and the translational evolution. Thus, v_0 and D_r are both relevant parameters for the active fluid. One way to describe ABP that is successful in the low-density limit is by assigning to the ABP system an effective temperature (or pressure) [32], based on the notion that a single ABP over long time and length scales undergoes diffusion with a renormalized diffusivity that in two spatial dimensions reads $D_{\mathrm{eff}} = D_t + (1/2)v_0^2/D_r$. Here, only a specific combination of v_0 and D_r enters. There are indications that the high-density dynamics of ABP on the contrary depends on both these parameters separately [18, 30, 31], because at high densities the average distance between ineracting particles is easily shorter than the persistence length associated to the swimming, $\ell_p = v_0/D_r$. It is therefore interesting to see the effect that varying both v_0 and D_r has on the stationary static structure.

The relevant dynamical rates of the AHS system thus are: the rate of passive Brownian diffusion, $\tau_0^{-1} = D_t/\sigma^2$, the rate of self-propelled motion, $\tau_v^{-1} = v_0/\sigma$, and the rate of active effective diffusion, $\tau_a^{-1} = v_0\ell_p/\sigma^2$. From these rates, three dimensionless parameters can be formed to quantify the amount of 'activity' in the system. (They are ratios of rates, and thus

called 'Péclet' numbers in analogy to hydrodynamic theory.) A natural choice from the equations of motion is the translational Péclet number that quantifies the rate of self propulsion in relation to passive diffusion, $\mathrm{Pe_t} = \tau_v^{-1}/\tau_0^{-1} = v_0\sigma/D_\mathrm{t}$. The low-density theory suggests to use the rate of active over that of passive diffusion, $\mathrm{Pe} = \tau_a^{-1}/\tau_0^{-1} = v_0^2/D_r D_\mathrm{t}$; at high densities one may expect the persistence length to play a crucial role, and thus the ratio of self-propelled motion relative to active difusion, $\mathrm{Pe_r} = \tau_v^{-1}/\tau_a^{-1}$. Note that $\mathrm{Pe_r}^{-1} = \ell_\mathrm{p}/\sigma$ is sometimes also referred to by the symbol Pe in the context of MIPS; we stick to the notation introduced in [32] to avoid confusion.

We thus compare the static structure factors obtained for the system at moderate density, $\eta = 0.2$, for various rotational diffusion coefficients, while keeping one of the three parameters ($\mathrm{Pe_t}$, Pe, or $\mathrm{Pe_r}^{-1}$) fixed. Varying D_r over two orders of magnitude shows (figure 9) that the static structure factors $S(q)$ are in fact independent on D_r in the regime of moderately strong self propulsion. The curves for different D_r fall on top of each other within error bars at fixed $\mathrm{Pe_t}$, with the exception of a small increase towards $q \to 0$. The latter indicates that the appearance of MIPS is influenced by both v_0 and D_r, while the dependence on D_r has no significant structural precursors in the fluid.

At fixed Pe (middle panel of figure 9), an increase in D_r has a similar effect as increasing v_0 regarding the change in nearest-neighbor structure that is reflected in the change of the peak positions in $S(q)$. A similar conclusion holds for the evolution of $S(q)$ with increasing D_r at fixed persistence length (right panel of the figure). Note that one expects the dynamics for $D_\mathrm{r} \to \infty$ at fixed v_0 to become identical to that of passive hard spheres, because in this limit the net effect of self propulsion vanishes. Figure 9 suggests that this is true only if the limit is taken such that the persistence length vanishes sufficiently quickly: only for the case of fixed $\mathrm{Pe_t}$, the structure factor approaches the passive one with increasing D_r at least at low q.

At high densities, the situation is less clear, because phase separation sets in at very different self-propulsion velocities for different D_r. Static structure factors for $\eta = 0.6$ and $\eta = 0.7$, shown in figure 10, confirm the observation made above: as long as the system remains in the homogeneous fluid state, D_r itself appears to have very little influence on the static structure. At fixed Péclet number or fixed persistence length, the increase of D_r does not render the system more passive-like, but rather induces a change in $S(q)$ that is similar to the one seen upon increasing v_0 at fixed D_r.

4. Conclusions

We have obtained static structure factors and radial distribution functions from simulations of active Brownian hard-disk fluids. The system remains in the homogeneous fluid phase for all packing fractions $\eta \lesssim 0.7$ and low enough activities, $v_0 \lesssim 12\, D_\mathrm{t}/\sigma$ for $D_\mathrm{r} = 1\, D_\mathrm{t}/\sigma^2$; it also remains a homogeneous fluid for low densities, $\eta \lesssim 0.2$, and all the self-propulsion velocities we have studied.

The evolution of the static structure factor with density, outside the region of MIPS, resembles that of the passive fluid at finite q. On the low-density side of the phase-separation spinodal, increasing activity causes the fluid to exhibit slightly more pronounced ordering concommittant with a shift of typical interparticle separations to smaller distances. For the active hard-disk system, the static structure evolves from the passive one to an essentially v_0-independent active one: the $S(q)$ data with increasing v_0 converge to a well-defined limiting curve.

The high-density fluid reveals an interesting non-monotonic change in $S(q)$ with increasing v_0. Small self-propulsion velocities destroy the ordering that is present in the passive dense fluid, but further increasing the self-propulsion velocity reinstitutes more pronounced ordering at a shorter average particle separation. This highlights the interplay of a nearest-neighbor length scale (that determines the fluid structure in equilibrium) and the length scale introduced by persistent swimming.

It is possible to qualitatively understand the active-fluid $S(q)$ by analogy to the effects caused by an attractive interaction in an equilibrium fluid. In particular the non-monotonic evolution of $S(q)$ at high densities suggests an effective attraction of a range that is around 10% of the particle diameter. From this, an interplay between the effective activity-induced attraction width and the interparticle separation length arises. In the equilibrium fluid, such an interplay causes non-monotonic changes in the dynamics that lead to a reentrant melting of the glass [28, 33]. Indeed, a similar reentrant behavior of the glassy dynamics of an active fluid (albeit not an ABP fluid) has been discussed [34]. It should, however, be stressed that the effective-attraction description of $S(q)$ does not acknowledge the non-equilibrium nature of the active fluid. While changes in the glassy dynamics of an equilibrum fluid are largely governed by changes in $S(q)$, the same need not be true for the ABP system.

The fact that activity enhances structural order in the low-density fluid might at first sight seem surprising: The single-particle dynamics of ABP can be mapped onto diffusion with an enhanced diffusivity, $D_\mathrm{eff} \geqslant D_\mathrm{t}$. This mapping suggests a description in terms of an enhanced effective temperature, and from such a mapping, one would expect the oscillations in $S(q)$ to become less pronounced. The qualitative mapping to an effective attraction, instead of an effective temperature, much better explains the observed changes in $S(q)$.

The effect of rotational diffusivity on the low-density static structure of the active hard-disk fluid is weak. At high densities, the influence of D_r is masked by the onset of phase separation, so that the trends emerging in $S(q)$ are less clear. As already known from studies of MIPS, it is not possible to maintain the high-density strongly active system in a homogeneous fluid state. Doing so may be possible in suitably polydisperse systems (either using size polydispersity or polydispersity in self-propulsion speed).

Our data can be used as a reference for future theoretical studies which construct approximative closures for the structure based on the Smoluchowski equation [8, 35, 36] or for mode-coupling-like dynamical theories that either need static

structure factor data as an input [29, 36, 37] or can in principle approximate it based on the equilibrium one [31]. As a remark, however, the extension of theoretical frameworks to calculate $S(q)$ and related structural quantities that characterize the non-equilibrium steady state of active particles is not obvious, even for radially-symmetric pair potentials. There are two basic reasons for that: first, active Brownian particles possess an internal orientational degree of freedom which represents the direction of their intrinsic motion. This orientational degree of freedom is irrelevant for spherical passive systems but similar to molecular liquids with rotational symmetric shape (such as rods). For these liquid-crystalline systems, it is much more difficult to derive and numerically solve integral equations closures to access the orientationally averaged structure factor for the particle centers [38–40]. Second, more importantly, active Brownian system are not in equilibrium which brings about complications in the description of the steady state.

Acknowledgments

We gratefully acknowledge funding from Deutsche Forschungsgemeinschaft (DFG) within the Special Priority Programme SPP 1726 'Microswimmers', grants VO 1270/7-2 and LO 418/17-2.

ORCID iDs

H Löwen https://orcid.org/0000-0001-5376-8062
Th Voigtmann https://orcid.org/0000-0002-1261-9295
F Smallenburg https://orcid.org/0000-0002-9401-6067

References

[1] Romanczuk P, Bär M, Ebeling W, Lindner B and Schimansky-Geier L 2012 *Eur. Phys. J.: Spec. Top.* **202** 1–162
[2] Elgeti J, Winkler R G and Gompper G 2015 *Rep. Prog. Phys.* **78** 056601
[3] Bechinger C, Di Leonardo R, Löwen H, Reichhardt C, Volpe G and Volpe G 2016 *Rev. Mod. Phys.* **88** 045006
[4] Buttinoni I, Volpe G, Kümmel F, Volpe G and Bechinger C 2012 *J. Phys.: Condens. Matter.* **24** 284129
[5] Howse J R, Jones R A L, Ryan A J, Gough T, Vafabakhsh R and Golestanian R 2007 *Phys. Rev. Lett.* **99** 048102
[6] Palacci J, Sacanna S, Kim S H, Yi G R, Pine D J and Chaikin P M 2014 *Phil. Trans. R. Soc.* A **372** 20130372
[7] Hansen J P and McDonald I R 2009 *Theory of Simple Liquids: with Applications to Soft Matter* 4th edn (Oxford: Elsevier) p 636
[8] Härtel A, Richard D and Speck T 2017 Microscopic structure in suspensions of active hard disks (arXiv:1708.01115)
[9] Cichocki B and Hinsen K 1990 *Physica* A **166** 473–91
[10] Löwen H 1994 *Phys. Rev.* E **50** 1232
[11] Scala A, Voigtmann Th and De Michele C 2007 *J. Chem. Phys.* **126** 134109
[12] Fily Y and Marchetti M C 2012 *Phys. Rev. Lett.* **108** 235702
[13] Cates M E and Tailleur J 2015 *Annu. Rev. Condens. Matter Phys.* **6** 219–44
[14] Bialké J, Speck T and Löwen H 2015 *J. Non-Cryst. Solids* **407** 367–75
[15] Zöttl A and Stark H 2016 *J. Phys.: Condens. Matter* **28** 253001
[16] Siebert J T, Letz J, Speck T and Virnau P 2017 *Soft Matter* **13** 1020–6
[17] Levis D, Codina J and Pagonabarraga I 2017 *Soft Matter* **13** 8113
[18] Ni R, Stuart M A C and Dijkstra M 2013 *Nat. Commun.* **4** 2704
[19] Bernard E P and Krauth W 2011 *Phys. Rev. Lett.* **107** 155704
[20] Thorneywok A L, Abbott J L, Aarts G A L and Dullens R P A 2017 *Phys. Rev. Lett.* **118** 158001
[21] Baus M and Colot J L 1986 *J. Phys.* C **19** L643–8
[22] Bialké J, Speck T and Löwen H 2012 *Phys. Rev. Lett.* **108** 168301
[23] Farage T F, Krinninger P and Brader J M 2015 *Phys. Rev.* E **91** 042310
[24] Ginot F, Theurkauff I, Levis D, Ybert C, Bocquet L, Berthier L and Cottin-Bizonne C 2015 *Phys. Rev.* X **5** 011004
[25] Mani E and Löwen H 2015 *Phys. Rev.* E **92** 032301
[26] Wittmann R and Brader J M 2016 *Europhys. Lett.* **114** 68004
[27] Bolhuis P, Hagen M and Frenkel D 1994 *Phys. Rev.* E **50** 4880–90
[28] Dawson K, Foffi G, Fuchs M, Götze W, Sciortino F, Sperl M, Tartaglia P, Voigtmann Th and Zaccarelli E 2001 *Phys. Rev.* E **63** 011401
[29] Berthier L 2013 *Phys. Rev. Lett.* **112** 220602
[30] Bi D, Yang X, Marchetti M C and Manning M L 2016 *Phys. Rev.* X **6** 021011
[31] Liluashvili A, Ónody J and Voigtmann Th 2017 *Phys. Rev.* E **96** 062608
[32] Takatori S C, Yan W and Brady J F 2014 *Phys. Rev. Lett.* **113** 028103
[33] Pham K N, Puertas A M, Bergenholtz J, Egelhaaf S U, Moussa A, Pusey P N, Schofield A B, Cates M E, Fuchs M and Poon W C K 2002 *Science* **296** 104–6
[34] Szamel G, Flenner E and Berthier L 2015 *Phys. Rev.* E **91** 062304
[35] Bialké J, Löwen H and Speck T 2013 *Europhys. Lett.* **103** 30008
[36] Farage T F F and Brader J M 2014 (arXiv:1403.0928)
[37] Szamel G 2016 *Phys. Rev.* E **93** 012603
[38] Gray C G and Gubbins K E 1984 *Theory of Molecular Fluids: Fundamentals* (*Int. Series of Monographs on Chemistry 9* vol 1) 1st edn (Oxford: Oxford University Press) p 626
[39] Klapp S H L and Patey G N 2000 *J. Chem. Phys.* **112** 3832–44
[40] Klapp S and Forstmann F 1997 *J. Chem. Phys.* **106** 9742–61